Improved Microseismic Event Hypocentre Location in Block Caving Mines using Local Earthquake Tomography

J.-Philippe. Mercier, Golder Associates, Canada (Seismologist, Montreal)

W. de Beer, Golder Associates, Canada (Principal, Montreal)

J.-Pascal Mercier, Advanced GeoScience Imaging Solutions, Canada

Abstract

In production data processing, event hypocentre locations are usually calculated by considering a homogeneous (constant) velocity within the volume of rock monitored. However, the rock mass is far from homogeneous and, in the block caving context, its state can change rapidly as caving progresses. The consequent large discrepancies between the homogeneous velocity approximation and the true velocity distribution can considerably hamper the characterization of cave induced microseismic activity. Local earthquake, or passive source, tomography provides an efficient way to estimate the 3D seismic velocity distribution and simultaneously refine estimates of microseismic event hypocentre locations. It is a robust inversion method that uses information readily available in the microseismic data. It requires no a priori knowledge of the rock mass composition and stress state and provides a comparatively easy way to estimate the 3D velocity distribution using only seismic data. We present the results of locating microseismic event hypocentres in a block cave using local earthquake tomography. In addition, the 3D velocity model(s) calculated provide information on the rock mass state and the distribution and evolution of stresses as caving progresses. We first use a synthetic example to demonstrate the method's ability to estimate the 3D seismic velocity distribution and simultaneously correct the hypocentre location. We then discuss results obtained using real data collected at a block caving operation.

1 Introduction

In hard rock mines, microseismicity provides useful information on the behaviour and response of the rock mass to mining. In block caving, it is recognized that the location and characteristics of microseismic events induced by mining could be used to better understand the evolution of the caving process and the overall rock mass response, both during the development of the undercut and extraction levels and during production. This has been put into practice at several block caves (e.g., H. White et al., 2004; Hudyma and Potvin, 2010a, 2010b) (Glazer and Hepworth, 2006; Glazer and Townsend, 2008; Glazer, 2008; Hudyma and Potvin, 2008; Hudyma et al., 2007a, 2007b; Potvin and Hudyma, 2008; Trifu et al., 2007; Hylton White et al., 2004). The amount and quality of information extracted from the microseismicity largely depends on the ability to accurately calculate the event hypocentre locations. In turn, the accuracy of the event hypocentre locations is directly related to how representative of reality the velocity model used to calculate the locations is: the more representative the model, the more accurate the location of the microseismic events.

In block cave mines (as in other type of mines), the event hypocentre locations are usually calculated by considering a homogeneous (constant) velocity within the volume of rock monitored. In the block caving context, the rock mass can be far from homogeneous, and its state can change rapidly as caving progresses. Potentially large differences between the homogeneous velocity used to calculate the event hypocentre locations and true velocities at different locations in the rock mass can considerably limit a microseismic monitoring system's ability to characterize cave-induced microseismic activity, yielding significant errors in

event hypocentre locations and source parameter calculations. For that reason, more sophisticated 3D heterogeneous velocity models that better represent the rock mass should be used.

Local earthquake, or passive source, tomography (LET) provides an efficient way to estimate 3D seismic velocity distributions and simultaneously refine estimates of microseismic event hypocentre locations. Compared to other approaches, LET provides an easy way to estimate the 3D velocity distribution employing only seismic data. It has been applied using mine-induced seismicity ((Huang et al., 2013; Maxwell and Young, 1996, 1993; Maxwell et al., 1998)). Our LET method is computation-efficient. It uses only readily available information collected from microseismic data, namely initial event hypocentre locations and P- and/or S-wave onset times. It requires no *a priori* knowledge of the rock mass composition or stress state.

We first verify the capabilities of this technique by applying it to a synthetic example. We then show how it can be applied to real data collected at a block caving mine during the caving process. Our results clearly show that our method helps to improve the accuracy of microseismic event hypocentre location estimates and obtain information on the 3D velocity distribution, yielding a better understanding of the rock mass state and the distribution and evolution of stresses as caving progresses. We show that LET provides an alternative to an approach that involves manual building of a 3D velocity model from available geotechnical information.

A note on terminology: by "location error" we mean the difference between a real source location and the calculated location for the same source. In practice, location errors can only be determined for synthetic sources, controlled sources (e.g., surveyed blasts or mechanically-induced vibrations) and mined-through induced or natural seismic event sources. "Location uncertainty" refers to a statistical measure of the size of error ellipsoid within which, to a high degree of confidence, the actual location of the source is. "Residual" or "travel time residual" refers to the goodness-of-fit measure employed in an inversion.

2 Method

The relation between arrival time, T_{ij}, velocity, $\mathbf{v}(\mathbf{x})$, and origin time, τ_{0i}, for an event i located at x_{ei} recorded at a sensor j located at x_{si} is as follows:

$$T_{ij} = \int_{L(\mathbf{v}(\mathbf{x}),\ \mathbf{x}_{e_i},\ \mathbf{x}_{s_j})} \mathbf{v}^{-1}(\mathbf{x})\ dl + \tau_{0i}, \tag{1}$$

Where $\int_{L(\mathbf{v}(\mathbf{x}),\ \mathbf{x}_{e_i},\ \mathbf{x}_{s_j})} \mathbf{v}^{-1}(\mathbf{x})\ dl$ represents the travel-time, t_{ij}, and $L(\mathbf{v}(\mathbf{x}),\ \mathbf{x}_{e_i},\ \mathbf{x}_{s_j})$ is the ray-path.

Equation 1 is non-linear, since the trajectory between a source i and a receiver j along which the seismic energy travels depends on the underlying velocity model, $\mathbf{v}(\mathbf{x})$, the event hypocentre location, $\mathbf{x}_{e_i}$ and the sensor location, $\mathbf{x}_{s_j}$, and since the calculated hypocentre location and event origin time depend on the velocity model.

The inverse problem consists in calculating simultaneously the 3D velocity distribution, event hypocentre location and event origin time corrections from travel-time measurements. To solve this inverse problem, we adopted a popular approach (e.g., Eberhart-Phillips, 1993, 1993; Kissling et al., 1994; Thurber and Eberhart-Phillips, 1999) consisting in linearizing Equation 1 and correcting the model parameters (velocities, event hypocentre locations and event origin times) to reduce the difference between the observed and predicted arrival times while imposing constraint on the resulting model in a series of linear inversions and forward modellings.

3 Synthetic Example

3.1 Synthetic Example Setting

The purpose of the synthetic test is to show that LET can recover complex velocity distributions and correct event hypocentre locations without any *a priori* knowledge of the velocity distribution. For the synthetic test, we built a 100x100x100 m^3 synthetic velocity model with a 20x20x20 m^3 cubic low velocity anomaly in the middle. We set the velocity of the background and the low velocity anomaly to 5,000 ms^{-1} and 1,000 ms^{-1}, respectively. We then distributed 25 sensors and 200 events inside the model but outside the low velocity anomaly using uniform and Gaussian random distributions, respectively. Figure 1 shows the synthetic velocity model, the location of sensors and the microseismic events.

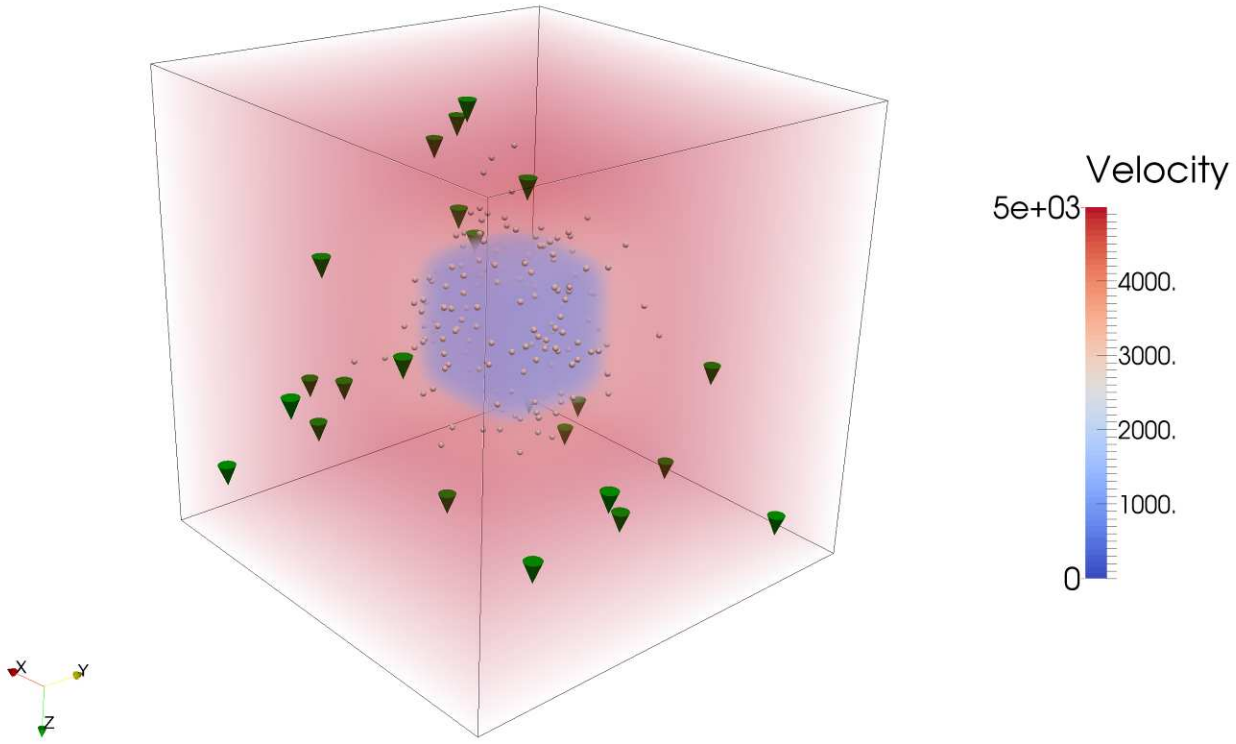

Figure 1: Oblique view of the synthetic velocity model. Blue and red represent low and high velocities, respectively. Inverse cones represent sensors and dots microseismic event hypocentre locations.

3.2 Synthetic Travel Time Data and Initial Event Hypocentre Locations

Using the settings discussed previously, we generated a set of synthetic travel times using a Fast Marching Eikonal solver (Sethian, 1999) along 40% of the all possible ray paths, which represents on average 10 travel times per event. Note that every event-sensor pair yields one ray path. Employing the synthetic travel times, we then calculated the event hypocentre locations in a homogeneous grid with a velocity of 5,000 ms^{-1}.

3.3 Inversion Setting

Joint velocity, event hypocentre and event origin time inversion was performed on the synthetic travel time data set. We used a homogeneous grid, with a velocity of 5,000 ms^{-1} as a starting velocity model and the event hypocentre locations calculated from the synthetic travel time on this homogeneous grid as the starting point for event hypocentre locations. The spacing of the inversion grid was set to 1 m in every direction, yielding a little more than 1 million grid nodes.

3.4 Synthetic Test Inversion Results

Figure 2a compares the true velocity profile and the velocity profiles obtained after 1, 10 and 50 iterations measured along the Z axis for X and Y constant and equal to 50 m (middle of the model). The recovered velocity model converges towards the true velocity. The mean relative error in percent ($\sum_n \frac{\mathbf{v}_\mathrm{T}(\mathbf{x}_n)-\mathbf{v}_\mathrm{R}(\mathbf{x}_n)}{\mathbf{v}_\mathrm{T}(\mathbf{x}_n)}/n \times 100$) between the true, $\mathbf{v}_\mathrm{T}(\mathbf{x})$, and recovered, $\mathbf{v}_\mathrm{R}(\mathbf{x})$, velocity model is 7%, 1.5% and 0.8% after 1, 10 and 50 iterations, respectively.

Figure 2b shows the evolution of the mean event hypocentre location error during the inversion process and compares the results to the mean location error for an event hypocentre located using the initial model homogeneous velocity (~10.5 m) and the true velocity model (~2 m). Note that a non-linear location procedure (Lomax et al., 2000) was used to locate the event hypocentre in the true velocity model. The mean error for the event hypocentre location calculated using LET decreases from approximately 10.5 m, the mean hypocentre location error in the homogeneous model, to slightly more than 3.5 m. The mean location error obtained after 50 iterations is roughly 1.5 m higher than the mean hypocentre location error calculated using the true model, and about 3 times smaller than the initial mean error for the event hypocentre located in the homogenous velocity model.

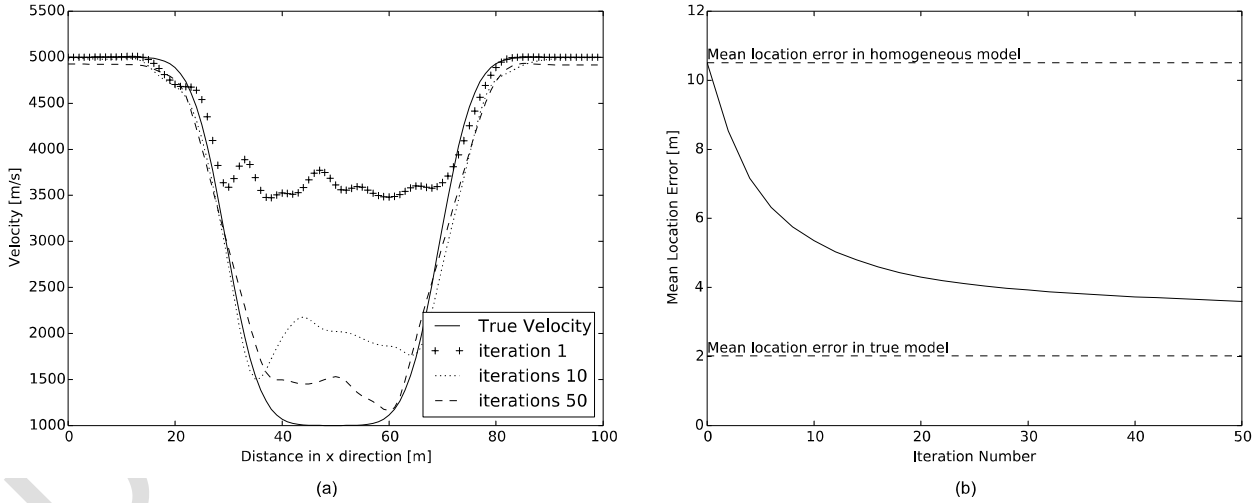

Figure 2: Comparison of original and recovered model parameters. (a) Velocity along the Z-axis for constant X and Y in the middle of the model at three stages of the inversion process. (b) Evolution of the mean event hypocentre location error during the inversion process.

4.0 Real Data Example: Block Caving

4.1 Context

We used a data set containing P-wave onset time measurements collected over a week at the height of seismic activity during production, and corrected the event hypocentre locations and event origin times.

4.2 Microseismic System

The microseismic activity at the mine was monitored by an array composed of 19 triaxial accelerometers and nine uniaxial geophones. The sensors were deployed relatively close to the ore body in a 3D geometry designed to ensure accurate detection and location of microseismic events throughout the caving process and to mitigate the shadowing effect expected from the growing cave.

4.3 Inversion Setting

The P-wave velocity models cover a volume extending over 550 m in the north and east directions and 500 m in the Z direction, fully encompassing the ore body being mined. The spacing between adjacent nodes was set at 5 m in every direction, yielding a model comprising 1.21 million nodes. The starting velocity model was chosen to be homogeneous (i.e., constant), with a velocity value of 3,900 ms^{-1} attributed to every node. This velocity corresponds to the average P-wave velocity obtained with calibration blasts. The inversions were performed independently on each of the velocity models, and 20 non-linear iterations were used. The regularization parameters were set to $1x10^{-13}$ and $1x10^{-7}$ for velocity and event hypocentre correction, respectively. These values were selected using a heuristic approach based on the so-called trade-off curve (see Rawlinson and Sambridge, 2003).

4.4 Inversion Results

Figure 3 presents the inversion results and shows in (a), the evolution of the cumulative travel time residual, (b), the difference in the estimated event hypocentre location uncertainty at the beginning and end of the inversion process, and (c), (d) and (e), three perpendicular cut-slices showing the resulting velocity models and the location of the corrected microseismic event hypocentres.

The inversion yielded a decrease in the cumulative travel time residual from the initial value of 0.65 ms to 0.25 ms at the end of the inversion process. Note that the cumulative travel time residual measures the fit between the predicted and observed travel times ($||t_{\mathrm{predicted}} - t_{\mathrm{observed}}||_2$). The event hypocentre location uncertainty, which is estimated from the covariance matrix, decreased from more than 30 m for events located in the homogeneous grid to approximately 10 m at the end of the inversion process. This represents a three-fold improvement.

In addition, the 3D seismic P-wave velocity distribution was calculated. The velocity model features a large, low velocity (blue) region surrounded by high velocity (red). The main low velocity region is located at the bottom, near the extraction level. The range of recovered velocity extends from approximately 2,900 ms^{-1} to 4,550 ms^{-1}, with a standard deviation of close to 150 ms^{-1}.

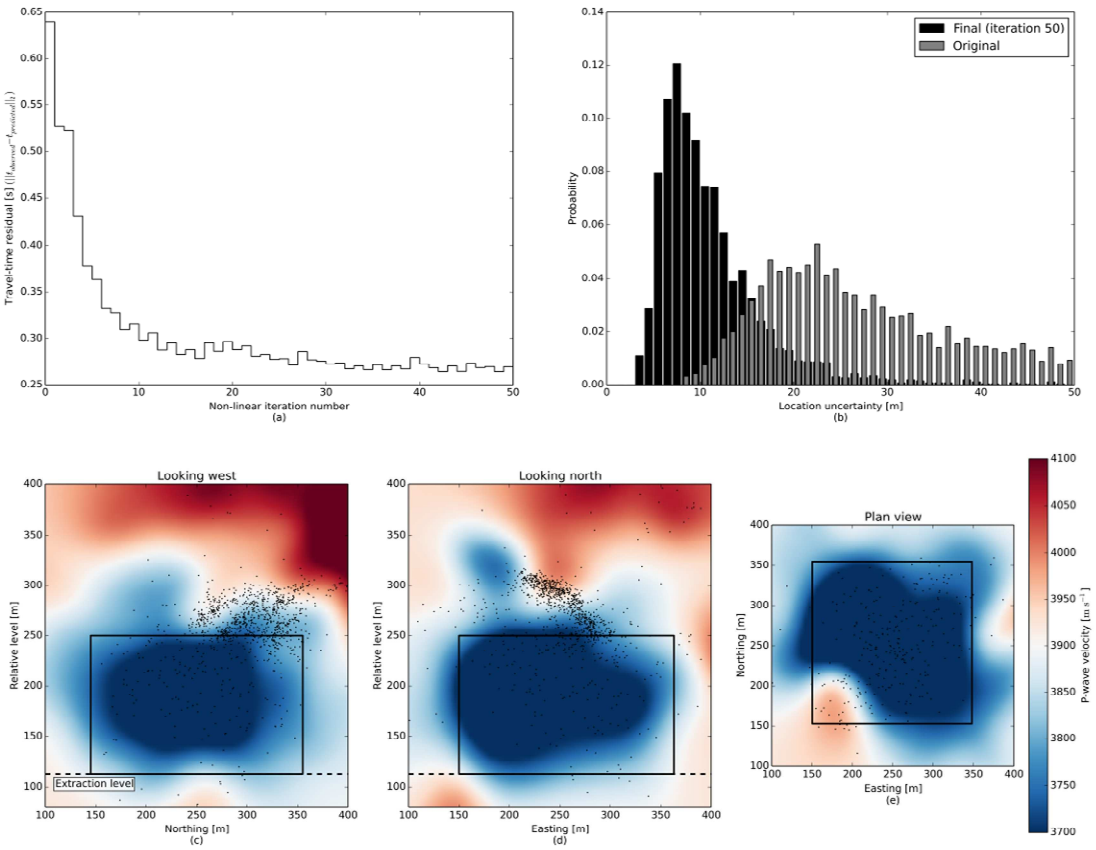

Figure 3: Tomographic inversion results for the period extending from 6 October 2004 to 13 October 2004. (a) Event hypocentre location uncertainty distribution at the beginning and at the end (after 50 non-linear iterations). (b) Travel-time residual evolution during the inversion process. (c), (d) and (e) Three perpendicular slices in the velocity model perpendicular to the east, north and z directions, respectively. The black rectangles give an indication of the volume encompassed by the cave during the time spanned by the data.

5 Discussion

The synthetic and real data examples presented in the previous sections show that LET can be used to significantly improve event hypocentre location in complex media with strong velocity contrast, using information readily collected by a microseismic monitoring system and without the need for explicit manual construction of a velocity model using estimates of cave geometry, rock mass properties, stress state and (simplified) geological units.

For the synthetic case, LET was able to reduce the location error by a factor of three compared to the homogeneous velocity model. In addition, the location error achieved by LET is only slightly higher than the smallest possible location error obtained using the true velocity model. In the case of the real data example, although the vast majority of location errors cannot be determined since the true locations of the microseismic events in question are generally not known, we have shown that the estimated location uncertainty was also improved by a factor of about three compared to the homogenous velocity model.

Apart from allowing relocation of the event hypocentre, LET images the 3D velocity distribution of the rock, providing insights into stress distribution and cave geometry. The velocity distribution can be used to supplement the geotechnical data collected during the caving process and provide insight into the rock mass

response to mining activity, the progression of the caving front and the geometry of the cave. When inversion is repeated for data sets covering different time periods, LET can also provide information on the variation of the 3D velocity distribution.

The explicit construction of a model representing the 3D velocity distribution during the caving process requires considerable logistics and adds to the burden of duties of a technical services department. Large amounts of geotechnical and geological data must be collected (generally manually), rapidly quality-controlled and then distributed and managed. To properly build a velocity model that is representative of the true rock mass velocity, precise information is required on rock mass properties, the caving front location, the cave geometry and the stress state of the rock mass. In addition, velocity models need to be updated regularly to account for the progression of the caving front, the changing cave geometry and stress redistribution around the cave. Even after this effort, with the best data quality and density, inaccuracies in the velocity model are inevitable.

6 Concluding Remarks

In this paper, we have demonstrated that local earthquake tomography (LET) can be used to improve the accuracy of event hypocentre location with very little information about the velocity model and no information on the cave geometry or stress state of the rock mass. We have applied LET to two data sets, one synthetic and one from a real block cave. Our results show that event location uncertainty can be significantly improved by using LET rather than homogeneous velocity models. An additional outcome of LET is a 3D velocity model that provides important insights on the rock mass response to mining, complementing other geotechnical data collected. In summary, our results show that LET can provide an alternative to an approach involving the manual building of a 3D velocity model from available geotechnical information.

References

Eberhart-Phillips, D., 1993. Local earthquake tomography: earthquake source regions. Seism. Tomogr. Theory Pract. 613–643.

Glazer, S., Hepworth, N., 2006. Crown pillar failure mechanism–case study based on seismic data from Palabora Mine. Min. Technol. 115, 75–84.

Glazer, S.N., 2008. Seismically active volume around the cave and its relation to the caving stages, in: MassMin 2008. Presented at the MassMin 2008 - 5th International Conference and Exhibition on Mass Mining, Luleå Sweden 9-11 June 2008, Luleå University of technology, Luleå Sweden, pp. 983–992.

Glazer, S.N., Townsend, P., 2008. The application of seismic monitoring to the future Lift 2 block cave at Palabora mining company, in: MassMin 2008. Presented at the MassMin 2008 - 5th International Conference and Exhibition on Mass Mining, Luleå Sweden 9-11 June 2008, Luleå University of technology, Luleå Sweden, pp. 919–930.

Huang, J.-W., Reyes-Montes, J., Young, R., 2013. Passive three-dimensional microseismic imaging for mining-induced rock-mass degradation, in: Rock Mechanics for Resources, Energy and Environment. CRC Press, p. 1000.

Hudyma, M., Potvin, Y., 2008. Characterizing caving induced seismicity at Ridgeway gold mine, in: MassMin 2008. Presented at the MassMin 2008 - 5th International Conference and Exhibition on Mass Mining, Luleå Sweden 9-11 June 2008, Luleå University of technology, Luleå Sweden, pp. 931–942.

Hudyma, M., Potvin, Y., 2010a. An Engineering Approach to Seismic Risk Management in Hardrock Mines. Rock Mech. Rock Eng. 43, 891–906.

Hudyma, M., Potvin, Y., 2010b. An Engineering Approach to Seismic Risk Management in Hardrock Mines. Rock Mech. Rock Eng. 43, 891–906.

Hudyma, M.R., Potvin, Y., Allison, D.P., 2007a. Seismic monitoring of the Northparkes Lift 2 block cave - part 1 undercutting, in: 1st International Symposium on Block and Sub-Level Caving Cave Mining. Presented at the 1st International Symposium on Block and Sub-Level Caving Cave Mining, The Southern African Institute of Mining and Metallurgy, Cape Town, pp. 303–334.

Hudyma, M.R., Potvin, Y., Allison, D.P., 2007b. Seismic monitoring of the Northparkes Lift 2 block cave - part 2 production caving, in: 1st International Symposium on Block and Sub-Level Caving Cave Mining. Presented at the 1st International Symposium on Block and Sub-Level Caving Cave Mining, The Southern African Institute of Mining and Metallurgy, Cape Town, pp. 335–354.

Kissling, E., Ellsworth, W., Eberhart-Phillips, D., Kradolfer, U., 1994. Initial reference models in local earthquake tomography. J. Geophys. Res. Solid Earth 1978–2012 99, 19635–19646.

Lomax, A., Virieux, J., Volant, P., Berge-Thierry, C., 2000. Probabilistic earthquake location in 3D and layered models. Mod. Approaches Geophys. 18, 101–134.

Maxwell, S., Young, R., 1993. A comparison between controlled source and passive source seismic velocity images. Bull. Seismol. Soc. Am. 83, 1813–1834.

Maxwell, S., Young, R., 1996. Seismic imaging of rock mass responses to excavation. Int. J. Rock Mech. Min. Sci. Geomech. Abstr. 33, 713–724.

Maxwell, S., Young, R., Read, R., 1998. A micro-velocity tool to assess the excavation damaged zone. Int. J. Rock Mech. Min. Sci. 35, 235–247.

Potvin, Y., Hudyma, M., 2008. Interpreting caving mechanisms using microseismic monitoring data, in: MassMin 2008. Presented at the MassMin 2008 - 5th International Conference and Exhibition on Mass Mining, Luleå Sweden 9-11 June 2008, Luleå University of technology, Luleå Sweden, pp. 971–982.

Rawlinson, N., Sambridge, M., 2003. Seismic traveltime tomography of the crust and lithosphere. Adv. Geophys. 46, 81–198.

Sethian, J.A., 1999. Fast marching methods. SIAM Rev. 41, 199–235.

Thurber, C., Eberhart-Phillips, D., 1999. Local earthquake tomography with flexible gridding. Comput. Geosci. 25, 809–818.

Trifu, C.-I., Shumila, V., Burgio, N., 2007. Characterisation of the Caving Front at Ridgeway Mine, New South Wales, Based on Geomechanical Data and Detailed Microseismic Analysis, in: Challenges in Deep and High Stress Mining. Australian Centre for Geomechanics, Perth, Australia, pp. 443–453.

White, H., de Beer, W., White, H., van As, A., 2004. Design and Implementation of Seismic Monitoring Systems in a Block-Cave Environment, in: MassMin 2004. Presented at the MassMin 2004 (2004 : Santiago, Chile), Santiagom Mineria Chilena, Santiago.

White, H., de Beer, W., White, H., van As, A., Allison, D., 2004. implementation of seismic monitoring systems in a block-cave environment. Presented at the Massmin 2004, Santiago, Chile, pp. 559–554.